15B.5

Azimuth-Frequency Analysis for Wind Farm Clutter Identification and Mitigation in Doppler Weather Radars

Jimeng Zheng, Bryan Perfetti, and M. Kaveh

Department of Electrical and Computer Engineering, University of Minnesota, Minneapolis, MN, Email: zheng088@umn.edu

Dr. Svetlana Bachmann, and Dr. Robert Monson

Lockheed Martin

1. INTRODUCTION

The rising cost of fossil fuels and the threat of global climate change have driven governments to actively pursue alternative ("green") energy sources (Isom et al. 2008). Among various kinds of "green" energy, wind energy is of special interest, due to its easy maintenance, relatively low long-term cost and the conducive geography of many areas. Thus, in recent years, wind energy production capacity in North America has maintained an annual rate of increase of more than 30% except in the 2010's (15%) (TheWindPower 2010). The U.S. Department of Energy has set a goal for wind energy to supply 20% of U.S. electricity consumption by 2030 (DOE 2008). Despite these advantages of wind energy, the construction of wind farms may be restricted partially because of severe interference with air traffic control, surveillance, and weather radar systems. Therefore, there has been recent interest in understanding the impact of turbine interference and the corresponding mitigation methods in radar systems.

The wind farms' interference on the surveillance radar systems was first noticed in Europe, e.g. (Butler and Johnson 2003)(Poupart 2003)(Greving et al. 2007)(Greving and Malkomes 2008). Some of these works focus on the mitigation solution for air surveillance radar (ASR) (Butler and Johnson 2003)(Perry and Biss 2007) or air traffic control (ATC) radar systems (Poupart 2003)(Webster 2005), and in (Butler and Johnson 2003), an estimated cost was given for the necessary modifications/upgrades in 30 ASRs. In contrast to the weather-surveillance-radar, which is the focus of this paper, the air-surveillance-radar faces the problem of detecting and tracking fast moving point targets with large Radar Cross Section (RCS). The detection of such large RCS targets is different from the detection of the echoes from distributed weather scatterers, especially under the interference from wind turbines. For the large RCS targets, many tracking dependent techniques, e.g. Plot and Track Filters, Track Initiation Inhibit, Sensitivity Time Control and etc., can be employed to identify and remove the turbine interference (Perry and Biss 2007). However, most of the mitigation methods for ASR and ATC are not disclosed as either proprietary or sensitive, and their detailed concepts are not easy to ascertain.

Despite of the non-transparency of the research works related to ASR, there are many publications, e.g. (Bachmann et al. 2010a)(Bachmann et al. 2010b)(Isom et al. 2008)(Nai et al. 2011), describing the details of the mitigation methods for weather surveillance radar systems. Because of the vast number of operational systems, 159 radars in the Next Generation Weather Radar (NEXRAD) network [http://www.roc.noaa.gov/WSR88D/About.aspx], the turbine interference on the weather Doppler radar systems has received intensive attention (Vogt et al. 2007b). Early researches and investigations, e.g. (Vogt et al. 2007a)(Kent et al. 2008)(Vogt et al. 2009), focused on the impact of the wind farm interference on the weather radars, especially concerning at the large RCS of the wind turbines and the potential techniques that radar operators may deploy to work around the wind turbine clutter. These works urged the communication and cooperation between the wind farm owners, developers and the radar surveillance stakeholders. Among radar surveillance stakeholders, Radar Operation Center (ROC) is a representative of the national weather radar surveillance. The Federal Aviation Administration (FAA) regulates the Obstruction Evaluation Process, in which wind farm developers must submit their proposals to FAA for the evaluation of potential impact on ATC. In the past, ROC has not been involved in these proceedings. Today ROC is contributing to the wind farm planning and has the ability to influence the decision process and to consequently reduce the wind turbine construction within the line-of-sight of the corresponding weather radars. Therefore, planning a wind farm in the vicinity of a weather radar may become unfavorable to the wind energy industry, because the proposal may not realize. In addition to providing online tools to assist the wind farm developers in planning the placement of the turbines, weather radar community established regulations to promote the coordination between the wind farm developers and the NEXRAD operators. To potentially loosen the constraints presented to the wind farm developers by weather radar surveillance stakeholder, the radar signal processing mitigation methods are explored. Such mitigation methods rely merely on the modifications/upgrades of the digital signal processing algorithms of the weather radars, cost less, and seem more practical and favorable than many other methods, e.g. terrain masking.

Raw radar signals are the sequences of the in-phase and quadrature-phase (I/Q) components of the radar echo voltage. Prior to becoming useful for the meteorological interpretation, I/Q data undergo extensive processing stages including digital signal processing, Doppler spectral processing, data quality and contamination assessment, and consequent filtering and mitigation of unwanted echoes. From the point of view of digital signal processing, the radar echoes from the turbines comprise of two parts, the stationary one and the Doppler-shifted one. The stationary part is mainly the echoes from the towers supporting the turbines. It appears as a narrow-band clutter centered at the Zero-Doppler-Frequency (ZDF) in the Doppler spectrum representation of the raw radar signal. Because of its narrow-band property, it can be suppressed by the conventional Ground-Clutter-Filters. The Doppler-shifted part, which we refer to as Non-Zero Doppler Frequency Component (NZDFC), is the echoes from the rotating blades and/or nacelles. In the Doppler spectrum representation, it occupies a large range (or sometimes the entire range) of the non-zero Doppler frequencies including those of the weather signals. At close ranges (range here is the distance between the radar and a wind turbine) the magnitude and the variance of most of the Doppler coefficients from wind turbines are usually larger than or at least on the same order of that of the weather Doppler coefficients. Consequently, it is very difficult for signal processing algorithms to recover the weather Doppler spectrum by using the data only from the contaminated resolution cells. Thus, one of the solutions is to exploit the large scale and continuity properties of the weather scatterers. This means that the weather returns should have similar characteristics across the neighboring resolution cells and occupy larger areas in the (Elevation-)Range-Azimuth domain than the wind farms.

In (Isom et al. 2008), a signal processing algorithm, which is referred to as Multiquadric Spectral Interpolation (MQSI) in this paper, was proposed to exploit such property. MQSI assumes that all the resolution cells are classified on clean and contaminated. Then, several clean cells surrounding the wind farm area are carefully selected. The Doppler coefficients from these cells are utilized to construct models using Multiquadric interpolation method, for the region covering both the selected and the contaminated resolution cells. The values of these models at the contaminated cells are used to replace the corresponding Doppler coefficients. (We refer readers to (Isom et al. 2008) for more details of MQSI). Through this interpolation scheme, MQSI was shown to have good performance in recovering the reflectivity, radial velocity, and spectrum width in the contaminated resolution cells. However, the identification of the contaminated resolution cells is not trivial because of the multi-path effect and the occasional halt of turbines. Further, it is not clear on how to choose the clean cells around the wind farm and a key parameter of the multiquadric interpolation method. These two choices are crucial to the computational complexity and the recovery performance of MQSI.

Another signal processing mitigation method, which we refer to as Range-Doppler Pixel Classification (RDPC), was proposed in (Nai et al. 2011). In contrast to the identification plus interpolation scheme of MQSI, the philosophy of RDPC is just to identify and remove the pure turbine Doppler coefficients, with the others untouched. In the Range-Doppler-Spectrum domain, for any fixed azimuth angle, RDPC seeks to classify the Doppler coefficients with three labels: weather (including both clean weather and contaminated weather), turbine and noise. Such classification is performed by exploiting the differences between weather signal and turbine signal in the aspects of the continuity of the power level in range and the spread of signal power in Doppler frequencies. After removing the Doppler coefficients that are classified as turbine, the spectrum moments (reflectivity, radial velocity and spectrum width) are estimated by using only the remaining Doppler coefficients. (We refer readers to (Nai et al. 2011) for details of RDPc). Compared to MQSI, RDPC has much smaller computational complexity and keeps the resolution capability of the original system, since it does not employ any interpolation technique. However, RDPC usually provides biased estimates of the reflectivity, which results from the untouched but contaminated weather coefficients.

In this paper, we first define the Azimuth-Doppler Spectrum (ADS) in Section 2. In Section 3, a digital-signal-processing based mitigation method is proposed. The method features an automatic detector of the wind turbine contamination (based on Azimuth-Doppler spectrum) and a bilinear interpolator. Experiment and simulation results are provided in Section 4. Finally, conclusions are made in Section 5.

2. Azimuth-Doppler Spectrum

A common weather radar system, such as NEXRAD, has a parabolic dish antenna. The dish is mechanically rotated and tilted to acquire data from a volumetric 360 degree coverage. The Volume Coverage Pattern (VCP) defines the elevation tilts and the scan specifics, such as Pulse Repetition Times (PRT), number of pulses for coherent processing in one radial, etc. When a dish radar is in a stare mode (not rotating), the radial of data would represent 1 azimuth. These data can be processed in time, Doppler and range dimensions. When a dish radar rotates, additional azimuth dimension can be used for processing. Because a mechanically rotating dish cannot stare at each azimuth separately, each pulse is transmitted at an increment of azimuth. Therefore, there is a great flexibility on how such data can be processed. Traditionally, signal processing algorithms implemented in weather Doppler radar systems calculate the Doppler spectrum of each resolution cell and then apply filtering or interpolation methods in the Range-Doppler plane. However, in this paper, we develop our algorithms based on the Azimuth-Doppler Spectrum (ADS), which is generated as follows. Suppose, at range gate R, the received complex I/Q signal $x_R(t)$ is from the azimuth angle θ_t with $t = 0, ..., T$, which is assumed to scan through the surveillance area with constant step size δ_θ. Further, assume that any successive $2W_H + 1$ samples are within one beam-width. Thus, centered at azimuth angle θ_t, all the samples between $x_R(t-W_H)$ and $x_R(t+W_H)$ are from the corresponding resolution cell. Here, we define the data vector for this resolution cell as

$$\mathbf{x}_R(\theta_t) = [x_R(t - W_H), x_R(t - W_H + 1), ..., x_R(t + W_H)]^T. \tag{1}$$

Then, by applying windowing technique in time domain, the corresponding complex Doppler spectra are defined as

$$B_R(\theta_t) = DFT(\mathbf{x}_R(\theta_t) \times \mathbf{w}),$$

and

$$X_R(\theta_t) = DFT(\mathbf{x}_R(\theta_t)),$$

where DFT stands for the Discrete-Fourier-Transform, $\mathbf{w} \in \mathbb{C}^{2W_H+1\times 1}$ is the Blackman window series and the multiplication between $\mathbf{x}_R(\theta_t)$ and $\mathbf{w}$ is in element-wise. By using the Blackman window, the magnitude of the Doppler coefficients of $B_R(\theta_t) \in \mathbb{C}^{2W_H+1\times 1}$ suffers less from the spectrum leakage and better represents the signal power of the corresponding frequency bins than that of $X_R(\theta_t)$. In contrast, $X_R(\theta_t) \in \mathbb{C}^{2W_H+1\times 1}$ uses the rectangular window and, therefore, has higher resolution and side-lobe level while keeping the phase information of the Doppler coefficients which is important to our detector. Both $B_R(\theta_t)$ and $X_R(\theta_t)$ are used in our detector and the bilinear interpolation is performed on $B_R(\theta_t)$.

Based on these definitions, the complex Azimuth-Doppler Spectrum is constructed as:

$$\mathbf{B}_R = [B_R(\theta_{W_H}), B_R(\theta_{W_H+1}), ..., B_R(\theta_{T-W_H})]^T,$$

and

$$\mathbf{X}_R = [X_R(\theta_{W_H}), X_R(\theta_{W_H+1}), ..., X_R(\theta_{T-W_H})]^T.$$

Note that the data samples used in $X_R(\theta_t)$ ($B_R(\theta_t)$) and $X_R(\theta_{t+1})$ ($B_R(\theta_t + 1)$) have $2W_H$-point overlapped. Further, by putting the ADS of all the range gates together, we can get three dimensional data sets:

$$\mathbf{B}(R, \theta, K) = \mathbf{B}_R(\theta, K),$$

and

$$\mathbf{X}(R, \theta, K) = \mathbf{X}_R(\theta, K).$$

3. Mitigation Method

In this section, we propose a mitigation method on the basis of an automatic turbine interference detector and linear interpolation. Similar as MQSI, this method works on the Range-Azimuth-Doppler domain. The dimension of Elevation was not considered and can be included to further improve the performance. We begin with the introduction of the turbine interference detector.

a. *Wind Turbine Detector*

Although the positions of the wind turbines are usually known to the weather radar system, it is a good practice to map the range gates affected by the wind turbine returns. The detection and identification of contaminated range gates is critical because the radar beam pointing and the multipath effects depend on the propagation of electromagnetic energy in the atmosphere. The propagation path varies and this variation causes the observable and unpredictable phenomenon - some resolution cells, which do not correspond to the true locations of wind turbines, register contaminated returns. While other resolution cells that are known to represent the locations contaminated by the echoes from turbines, may become less affected - a beam propagation path may be higher, a turbine may turn away in a favorable angle and/or stop rotating by any reason, etc. In such cases, even the echoes from the cells, which are known to have turbines, may temporarily contain no NZDFC and, therefore, the application of mitigation methods in such cells is unnecessary and even harmful. On the basis of the ground clutter detector of Warde and Torres (2009), we introduce an adaptive wind turbine interference detector. This adaptive detector does not depend on the prior knowledge of turbines locations and works in the Azimuth-Doppler domain rather than the Range-Doppler domain of RDPC.

As in (Warde and Torres 2009), we assume that any successive $2W_H+2$ data samples are Wide-Sense Stationary (WSS) and define the cross spectrum $C_R(\theta_t)$ and its phase vector $P_R(\theta_t)$ as

$$C_R(\theta_t) = X_R(\theta_t) X_R(\theta_{t+1})^*, \tag{2}$$

and

$$P_R(\theta_t) = angle[C_R(\theta_t)],$$

where * denotes the conjugate operation, the vector multiplication is in element-wise and each element of $P_R(\theta_t)$

is the phase (in radius) of the corresponding element of $C_R(\theta_t)$. After some manipulation, we can rewrite (2) as

$$C_R(\theta_t)_k = e^{\frac{-j2\pi k}{2W_H+1}}[X_R(\theta_t)_k\Delta_t^* + |X_R(\theta_t)_k|^2], \qquad (3)$$

where $C_R(\theta_t)_k$ and $X_R(\theta_t)_k$ are the k^{th} elements of $C_R(\theta_t)$ and $X_R(\theta_t)$ respectively, and

$$\Delta_t = x_R(t+1+W_H) - x_R(t-W_H). \qquad (4)$$

Assume that the pass-band of the dominating signals ranges from the frequency index k_l to k_h. When $k_l \le k \le k_h$, $|X_R(\theta_t)_k|$ is much larger than the magnitude of Δ_t and, therefore,

$$C_R(\theta_t)_k \approx e^{\frac{-j2\pi k}{2W_H+1}}|X_R(\theta_t)_k|^2.$$

Thus, $P_R(\theta_t)_k \approx -2\pi k/(2W_H+1)$. When $k < k_l$ or $k > k_h$,

$$C_R(\theta_t)_k \approx e^{\frac{-j2\pi k}{2W_H+1}}X_R(\theta_t)_k\Delta_t^*,$$

and

$$P_R(\theta_t)_k \approx \frac{-2\pi k}{2W_H+1} + angle[X_R(\theta_t)_k] - angle[\Delta_t],$$

which is biased from $-2\pi k/(2W_H+1)$. Here we define a linear phase line which is $L_k = -2\pi k/(2W_H+1)$ for $k = -W_H, ..., W_H$. Then, by using a threshold on the difference between $P_R(\theta_t)_k$ and L_k, we can detect the Doppler coefficients in the pass-band of the dominating signals. Compared to the convention detector which is simply a threshold on the magnitude of the coefficients, this detector is more robust to the leakage from the strong stationary (low-frequency) signals because it operates on the phase of the coefficients. Furthermore, by combining this phase-based detector with the conventional one, we can improve the detection performance in identifying the pass-band of the dominating signals. We refer to this new detector by Phase Difference Detector (PDD) and formally state it here

If $|P_R(\theta_t)_k - L_k| < \tau_P$ and $|B_R(\theta_t)_k| > \tau_M$, then $F_R(\theta_t)_k = 1$, otherwise $F_R(\theta_t)_k = 0$,

where $B_R(\theta_t)_k$ is the Doppler coefficient obtained with Blackman Window, $F_R(\theta_t)_k$ is the flag of detection for the corresponding coefficient and τ_P and τ_M are the thresholds on the phase difference and the magnitude respectively.

Comparing the shapes of the Doppler power spectra representative for signal from weather, stationary clutter and rotating turbine blades, we observed that the signal power of turbine echoes is usually spread across the entire spectrum, unlike the signal power of weather and stationary clutters which just occupy relatively narrow bands of frequencies. Therefore, in contrast to RDPC, which classifies the Doppler coefficients individually, we choose to classify all the Doppler coefficients from resolution cell (R, θ_t) as contaminated or uncontaminated. Specifically, for each resolution cell (R, θ_t), we first apply PDD to detect the non-trivial coefficients (which are inside the pass-bands of either weather, clutter or wind turbines) and next compare $\sum_{k=1}^{2W_H+1} F_R(\theta_t)_k$ to a threshold (or equivalently, we can use a threshold, τ_I, on $\sum_{k=1}^{2W_H+1} F_R(\theta_t)_k/(2W_H+1)$). If the sum is above the threshold, then all the Doppler coefficients within this resolution cell are identified as contaminated. Note that we apply this detector for each (R, θ_t) and, therefore, there are overlaps among the resolution cells. In Section 4, examples are shown to illustrate the effectiveness of this detector.

b. Linear Interpolation

By applying PDD, we pinpoint the resolution cells contaminated by wind turbines. To reduce the impact of spectrum leakage, we now turn to the three dimensional data set $\mathbf{B}(R, \theta, K)$. Then, the mission of mitigating turbine interference reduces to recovering such Doppler coefficients in the contaminated cells. Since the strong stationary Doppler coefficients in such cells can have significant impact on the recovery of the spectral moments, especially the reflectivity and radial velocity, it is necessary to apply a ground clutter filter, e.g. Gaussian Model Adaptive Processing (GMAP), to every resolution cell before the interpolation process. Although the interpolation process can be accomplished by using MQSI, we choose to use simple bilinear interpolation for its lower computational complexity and parameter-free property.

Suppose that $S_C = \{(R_{t_j}, \theta_{t_j}), j = 1, ..., J\}$ is the set of the resolution cells that are detected by PDD as contaminated. Then, all the coefficients $\mathbf{B}(R_{t_j}, \theta_{t_j}, :)$ are notched and we define $\mathbf{B}_K(R, \theta)$, for each frequency index K,

$$\mathbf{B}_K(R, \theta) = \mathbf{B}(R, \theta, K).$$

Since the three important spectral moments (reflectivity, radial velocity and spectrum width) can be calculated merely from the power of the Doppler coefficients, we focus on $|\mathbf{B}_K(R, \theta)|$, and ignore the phases of these coefficients. By treating $|\mathbf{B}_K(R, \theta)|$ as an image with some missing pixels, we can fill in those notched coefficients by employing the bilinear interpolation algorithm. Since the bilinear interpolation is very standardized, we omit its details and make two comments on our mitigation method here. First, in contrast to RDPC, this new method also notches the contaminated weather coefficients and uses the interpolated values to replace them. Therefore, it can possibly achieve the recovery of all the three spectral moments at the same time. Second, although the infrastructure of this method is very similar to that of MQSI, it features an automatic turbine interference detector, PDD, and the computationally efficient linear interpolation which does not depend any parameter and prior information/selection. Several examples are shown in Section 4 to illustrate the performance of this new mitigation method.

4. EXPERIMENTAL RESULTS

In this section, we first apply the proposed Phase Difference Detector (PDD) and the bilinear interpolation method to the data sets obtained at Dodge City Kansas (KDDC) 2006. These data sets contain the I/Q or Level I data recorded from the corresponding WSR-88D radars and composed of turbine echoes with no weather, in clear air conditions. Then, because of the lack of weather data contaminated by returns from wind turbines, we turn to the synthetic data set. This data set were used by RDPC (Nai et al. 2011) and several related papers, and it is constructed by adding weather signal time series with turbine time series. This arrangement gives us the ground truth to evaluate the performance of the methods (Nai et al. 2011). In these examples, we use the Azimuth-Doppler spectra at the contaminated range gates to show the detection and spectrum recovery performance of PDD and the interpolation scheme.

a. KDDC Data Set

In Figure 1 is the reflectivity display of the KDDC data set. As shown in Figure 1, the wind farm is located at the resolution cells with range gates from 140 to 180 and azimuth angle from 240° to 255°, and there is no obvious weather clutter around the wind farm.

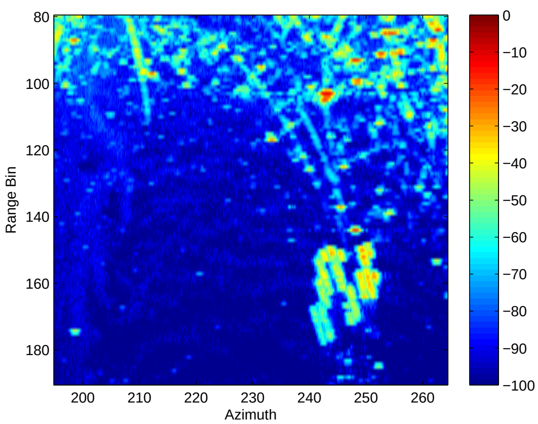

FIG. 1. (KDDC) Reflectivity Display

In Figure 2 and Figure 3, we take range gate 155 and 160 as examples and show the effectiveness of PDD. The top sub-figures of Figure 2 and Figure 3 are the Azimuth-Doppler spectra of these range gates. The center and the bottom sub-figures of Figure 2 and Figure 3 are the coefficients detected by PDD and their number versus azimuth, respectively. As shown by these figures, at range gate 155 and 160, the wind turbine contamination appears in two and three sectors of azimuth angles respectively, and, by setting threshold τ_I at around 0.4, PDD not only detectes the contaminated azimuth angles but also leaves the gaps separating those contaminated sectors un-detected, which keeps the weather information and is very important to the afterwards interpolation.

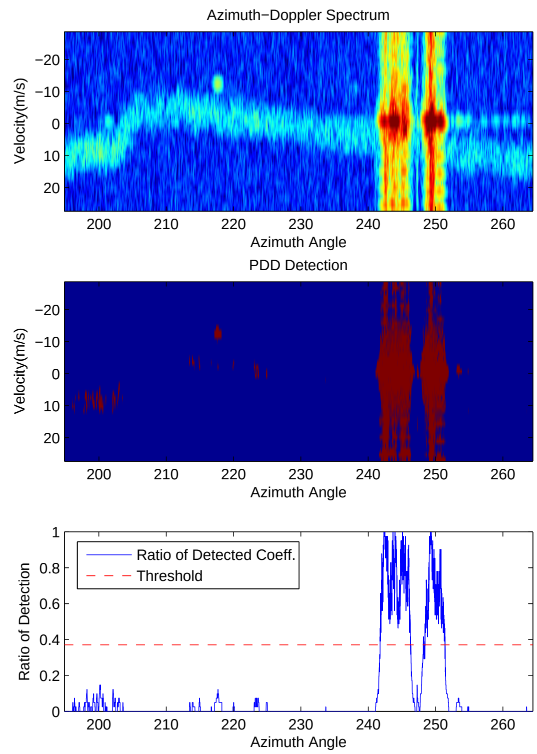

FIG. 2. (KDDC) Azimuth-Doppler Spectrum: Range Gate 155

We apply PDD using different τ_I to each range gates and show its results in Figure 4 ($\tau_I = 0.18$) and Figure 5 ($\tau_I = 0.4$). Figure 4(a) and Figure 5(a) are the generated wind turbine clutter masks (maps) with the red points representing the identified resolution cells with turbine contaminations, and, the reflectivity displays with the identified resolution cells notched are shown in Figure 4(b) and Figure 5(b) respectively. We can see that, in both of these settings, most of the resolution cells known to contain wind turbines are successfully detected by PDD, though moderate number of false alarms are present. However, around the wind farms, there are some resolution cells, which are of remarkably smaller reflectivity than the wind farms, are not detected by PDD. When τ_I is smaller (e.g. 0.18), the number of such cells is smaller (than $\tau_I = 0.4$) but the number of false alarms becomes bigger. Although in this case these cells affect the recovery/interpolation performance

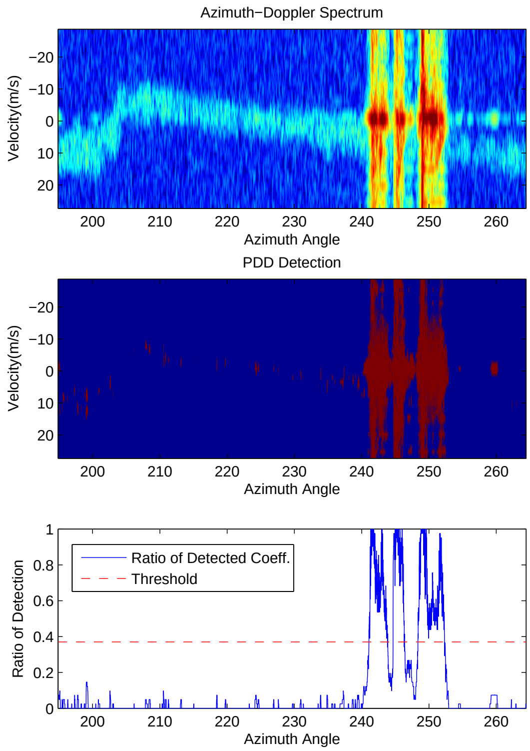

FIG. 3. (KDDC) Azimuth-Doppler Spectrum: Range Gate 160

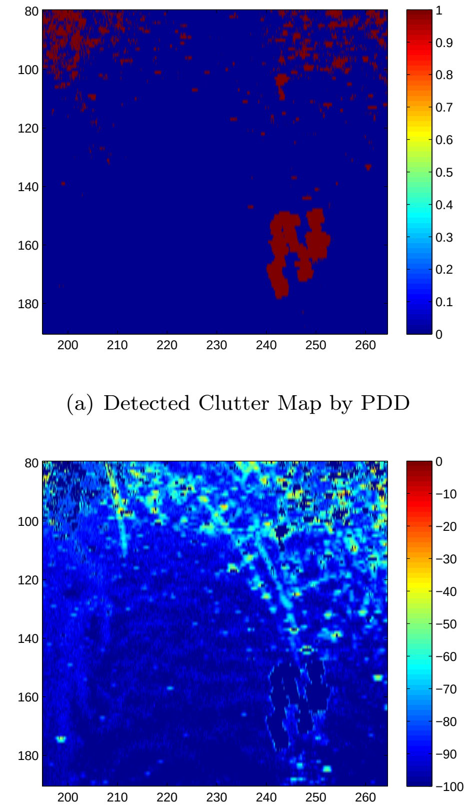

(a) Detected Clutter Map by PDD

(b) Notched Reflectivity Display

FIG. 4. (KDDC) PDD Results with $\tau_I = 0.18$

(as shown in next paragraph), they generally do not have severe impact in the cases of interest where the weather clutter is around or covering the wind farm.

Since in this data set there are no ground clutters beside or around the wind farm, we do not employ any ground clutter filter and directly apply the bilinear interpolation on the Doppler spectra. Figure 6, 7 and 8 shows the interpolated reflectivity display, Azimuth-Doppler spectra at range gates 155 and 160 respectively. According to these figures, the reflectivity displays for these two τ_Ts are very similar, but the recovery of the Azimuth-Doppler Spectrum of $\tau_I = 0.18$ seems better than that of $\tau_I = 0.4$. This is because, compared to $\tau_I = 0.4$, $\tau_I = 0.18$ causes PDD to detect more resolution cells surrounding the wind farm, which have stronger signal strength than the uncontaminated cells in neighborhood area of the wind farm (which are basically noise cells), and thus, by notching more such cells, $\tau_I = 0.18$ leads to smaller interpolated Doppler coefficients and better Azimuth-Doppler spectra.

b. Synthetic Data Set

In this subsection, we present the results of the afore mentioned synthetic data. Figure 9(a), 9(b) and 9(c) show the reflectivity displays of weather data, turbine data and the combined data (weather+turbine). As shown, the turbine data is obtained at clear air condition and is remarkably stronger than the weather, which causes obvious biases in the estimate of the reflectivity, radial velocity and spectrum width (shown in the last paragraph of this subsection).

Then, we apply the PDD to the combined data with $\tau_I = 0.35$, and show the results for range gates 155 and 165 in Figure 10 and 11 respectively. According to these two figures, PDD can correctly distinguish the contaminated resolution cells and the gaps between them, while make many false alarms in the resolution cells of pure weather signal. As shown later in this subsection, because of the spatial continuity of the weather signal, these false alarms does not have severe impact on the performance of the mitigation method. In Figure 12 are the detected clutter map and the reflectivity display with the detected cells notched. Similar as in Figure 10 and 11, there are many resolution cells of pure weather signal are classified as contaminated by PDD.

In this case, we use a simple group clutter filter (which

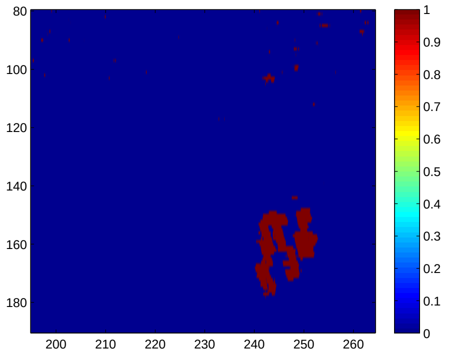

(a) Detected Clutter Map by PDD

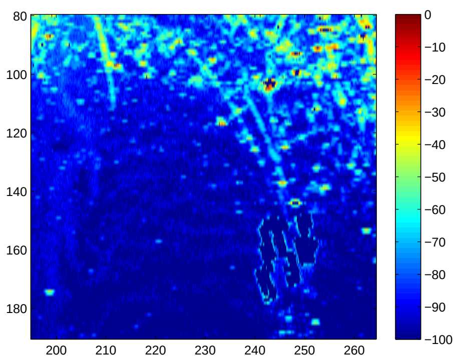

(b) Notched Reflectivity Display

Fig. 5. (KDDC) PDD Results with $\tau_I = 0.4$

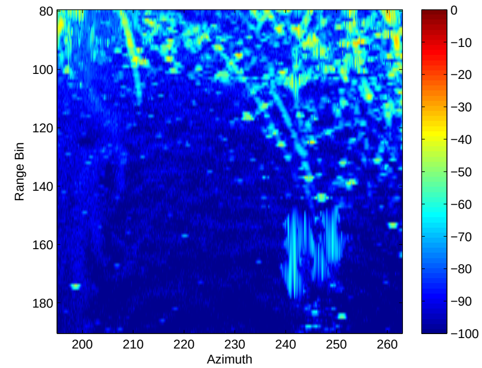

(a) Interpolation Result with $\tau_I = 0.18$

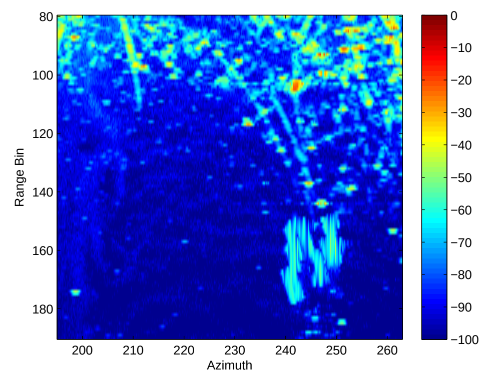

(b) Interpolation Result with $\tau_I = 0.4$

Fig. 6. (KDDC) Reflectivity: Interpolation Result

keeps the phase of the stationary coefficients and scale it by the magnitude of randomly picked High-Frequency Doppler coefficients) to remove the stationary signals in every resolution cell before the interpolation process. To have fair comparison, we also use PDD to detect the contaminated resolution cells for MQSI and all the parameters are independently and empirically chosen. In Figure 13, 14 and 15, we show the displays of reflectivity, radial velocity and the spectrum width of pure weather data (sub-figures (a)), the proposed method (sub-figures (b)), RDPC (sub-figures (c)) and MQSI (sub-figures (d)), respectively. As shown by Figure 13, all the three methods exhibit similar performance in recovering reflectivity. However, according to Figure 14 and 15, the proposed method has better performance than the other two in recovering radial velocity and spectrum width. This is because, first, RDPC misses many pure turbine coefficients which do not have remarkable effect on reflectivity but severely degrades the estimation of radial velocity and spectrum width. Second, for MQSI, PDD may miss some contaminated resolution cells, which have relatively very weak turbine signals, and these cells affect the model construction process of MQSI, which leads to degraded performance in recovering radial velocity and spectrum width. For better illustration, we also show the Azimuth-Doppler spectra of the interpolation results in the range gates 155 and 160 in Figure 16 and 17 respectively.

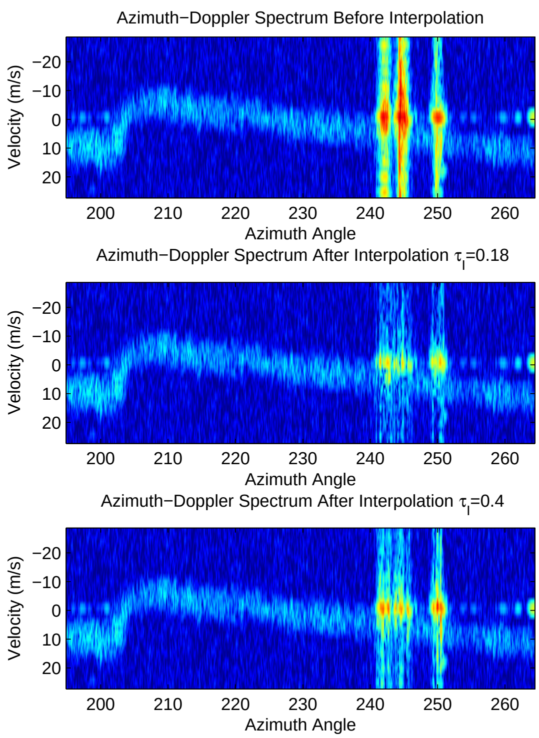

Fig. 7. (KDDC) Azimuth-Doppler Spectrum After Interpolation: Range Gate 155

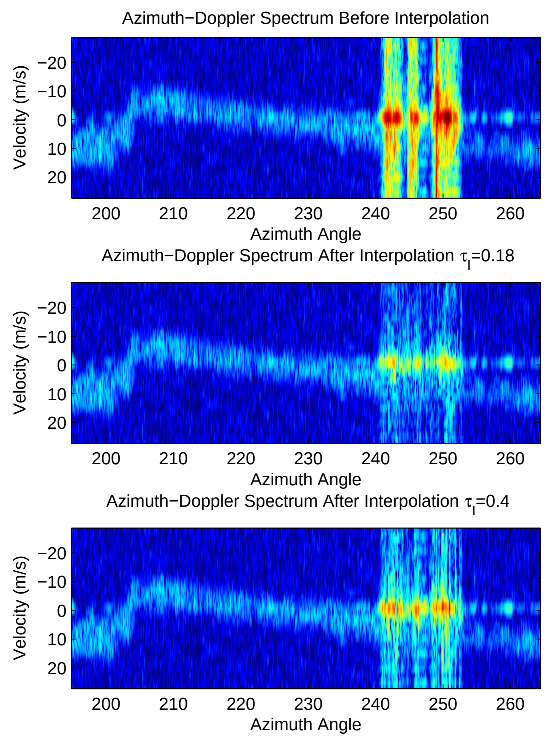

Fig. 8. (KDDC) Azimuth-Doppler Spectrum After Interpolation: Range Gate 160

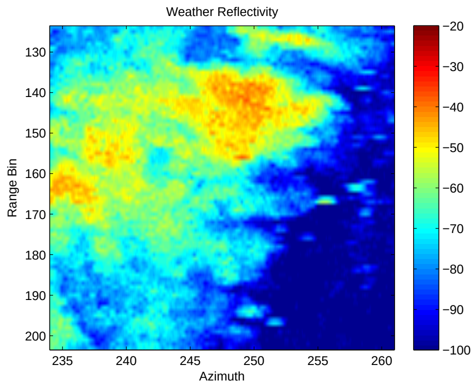

(a) Reflectivity: Weather Data

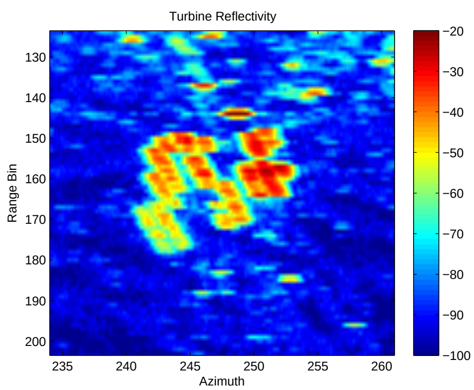

(b) Reflectivity: Turbine Data

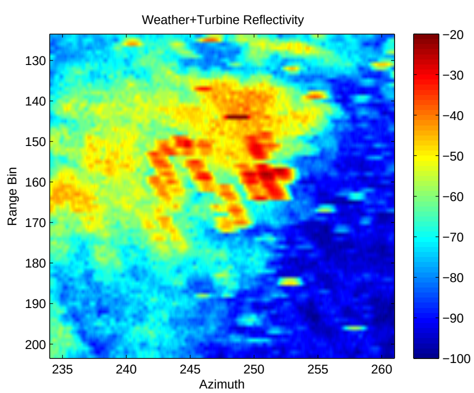

(c) Reflectivity: Weather+Turbine Data

FIG. 9. (SYNTHETIC) Reflectivity of Original Data

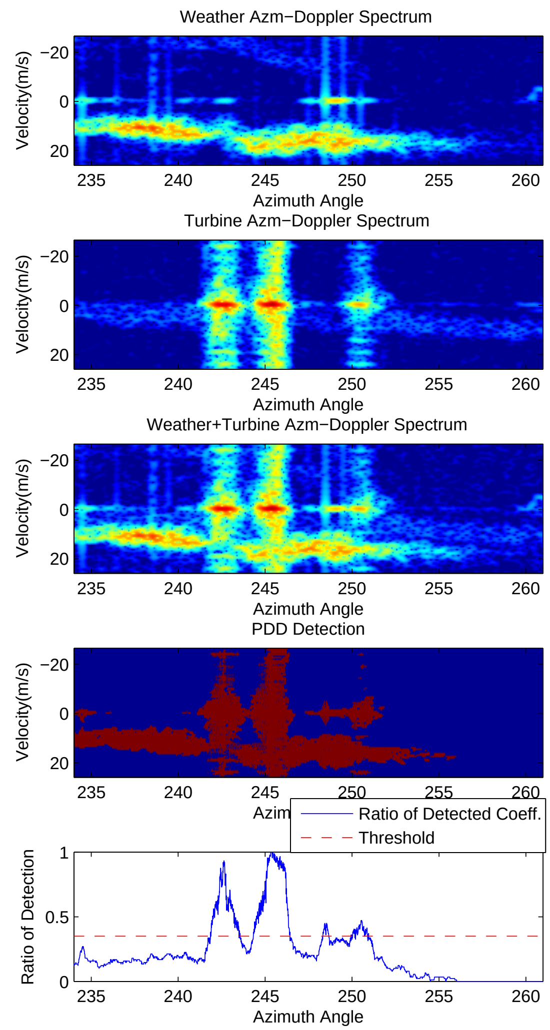

FIG. 10. (SYNTHETIC) Azimuth-Doppler Spectrum: Range Gate 155

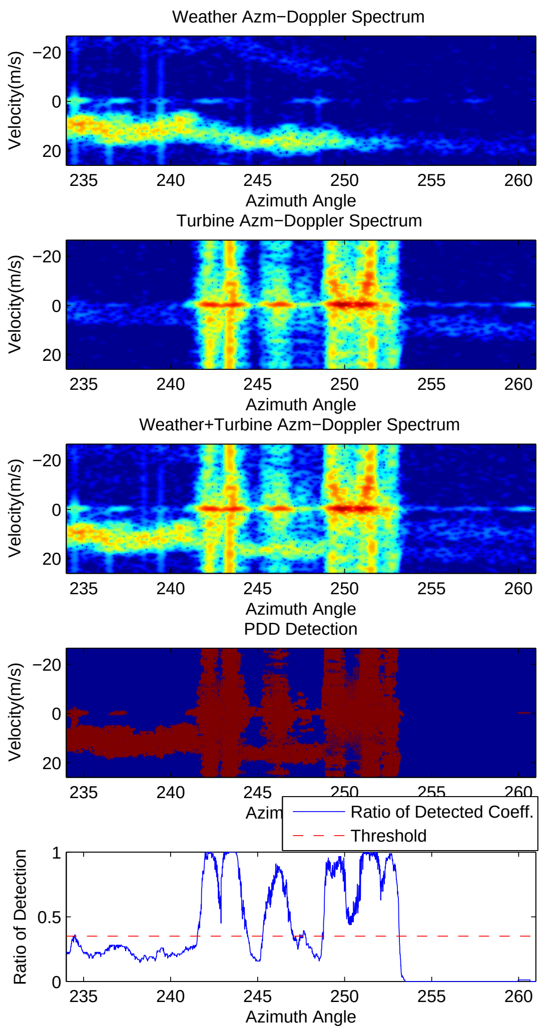

Fig. 11. (SYNTHETIC) Azimuth-Doppler Spectrum: Range Gate 160

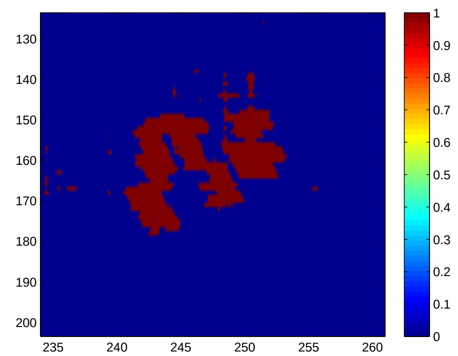

(a) Clutter Map by PDD

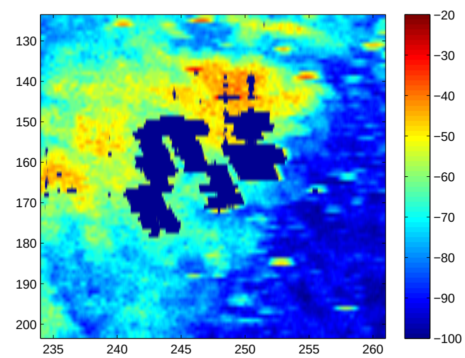

(b) Reflectivity Display with Detected Cells Notched

Fig. 12. (SYNTHETIC) PDD Results

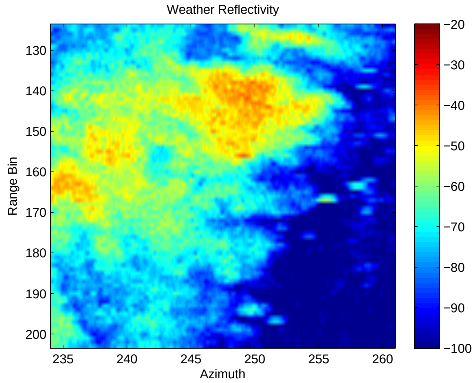

(a) Reflectivity: Weather Data

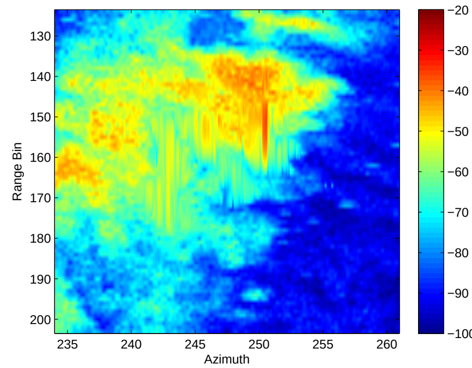

(b) Reflectivity: Result of Proposed Method

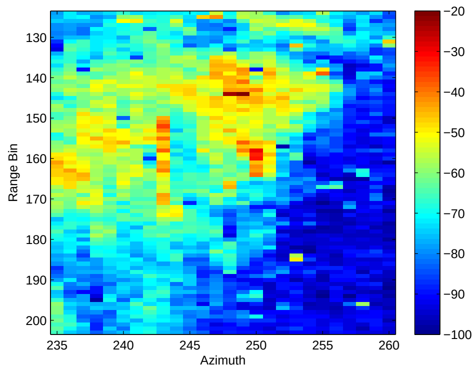

(c) Reflectivity: Result of RDPC

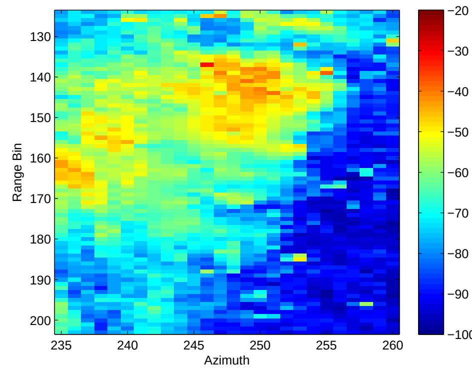

(d) Reflectivity: Result of MQSI

Fig. 13. (SYNTHETIC) Reflectivity

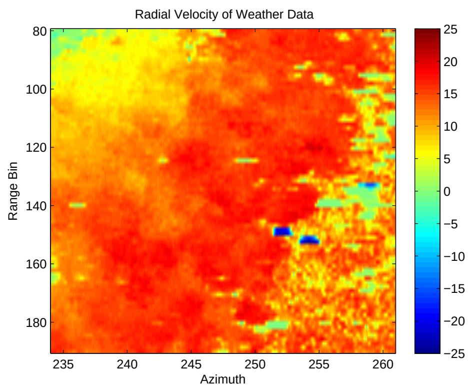

(a) Radial Velocity: Weather Data

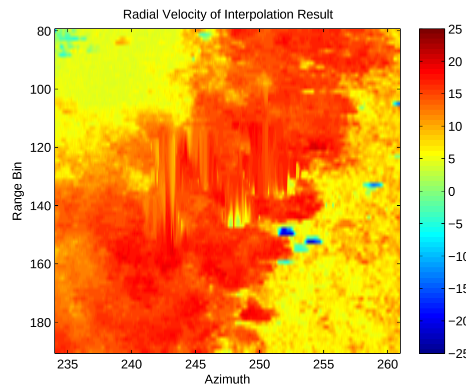

(b) Radial Velocity: Result of Proposed Method

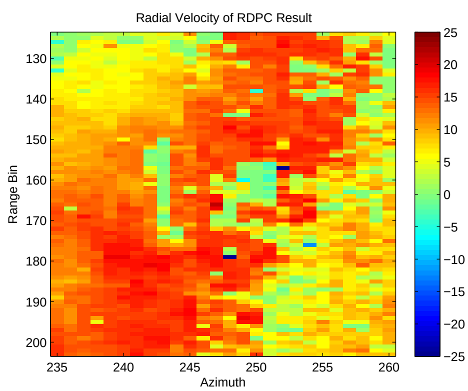

(c) Radial Velocity: Result of RDPC

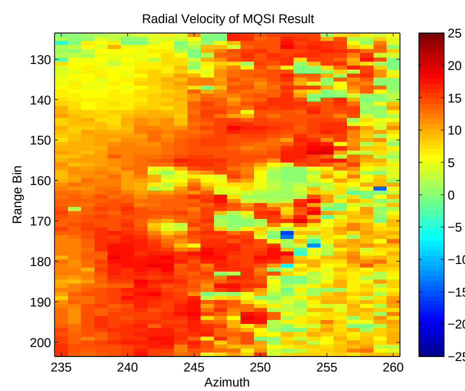

(d) Radial Velocity: Result of MQSI

Fig. 14. (SYNTHETIC) Radial Velocity

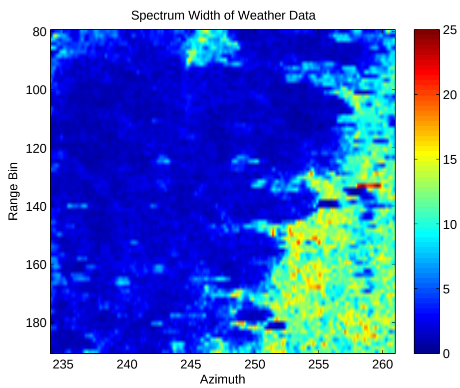

(a) Spectrum Width: Weather Data

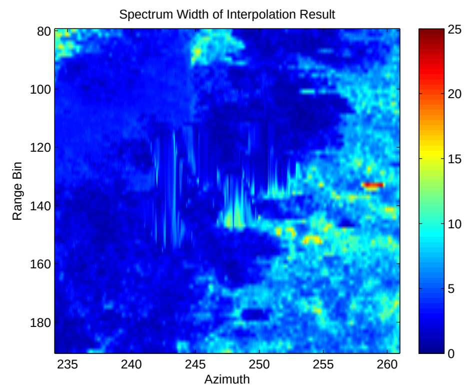

(b) Spectrum Width: Result of Proposed Method

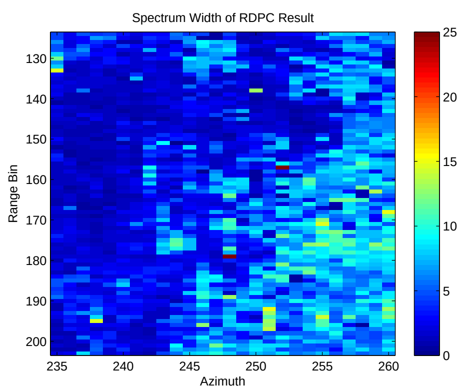

(c) Spectrum Width: Result of RDPC

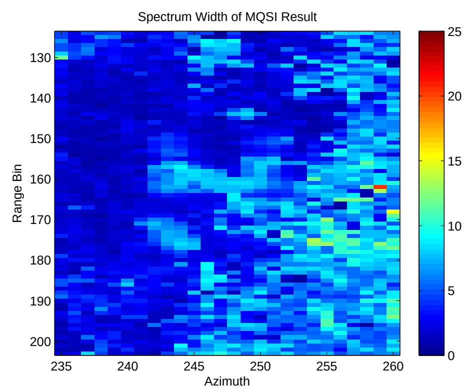

(d) Spectrum Width: Result of MQSI

Fig. 15. (SYNTHETIC) Spectrum Width

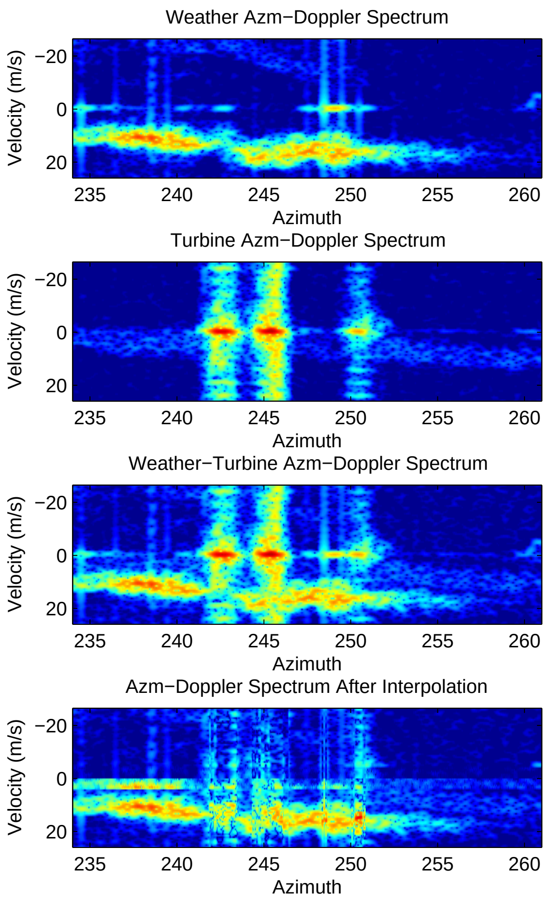

FIG. 16. (SYNTHETIC) Azimuth-Doppler Spectrum After Interpolation: Range Gate 155

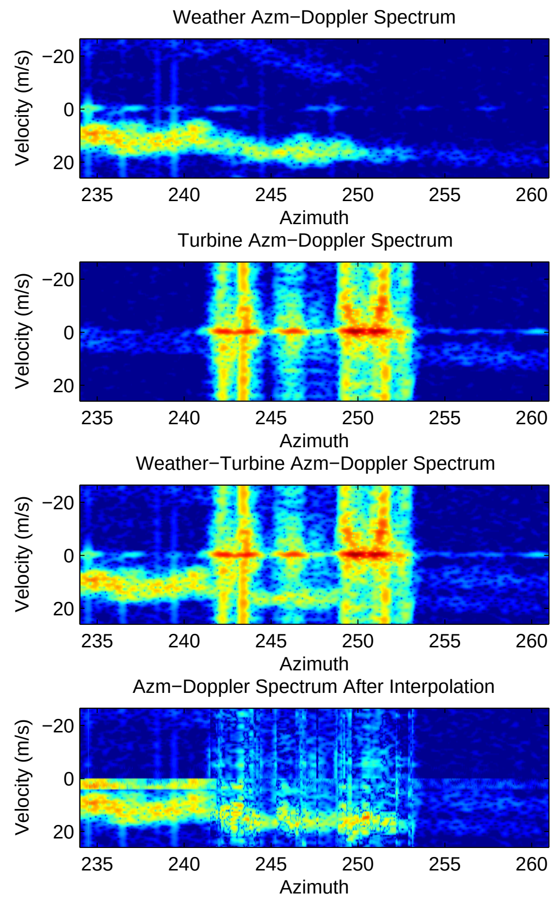

FIG. 17. (SYNTHETIC) Azimuth-Doppler Spectrum After Interpolation: Range Gate 160

5. CONCLUSION

In this paper, an automatic detector of wind turbine interference and a mitigation method of signal contamination have been proposed. Identification of Wind Turbine Clutter (WTC) independent of weather is based on relative attributes of the evolutionary Azimuth-Doppler spectrum coefficients and cross-spectral analysis of successive azimuth frames. Mitigation of WTC-corruption is carried out by nulling the contaminated Doppler spectra, followed by bi-linear interpolation on planes in the azimuth-range-Doppler 3D data set. The data used in the course of the investigation consisted of NEXRAD Level 1 scanning and synthetic Doppler weather radar returns. With comparison to the methods proposed in (Isom et al. 2008) and (Nai et al. 2011), promising results are demonstrated on the aforementioned measured and synthetic data.

6. ACKNOWLEDGEMENTS

The authors express their appreciation to Dr. Tim Crum, NOAA, and Prof. Robert Palmer, University of Oklahoma, for providing the measured data used in this study. This work was supported by the US Department of Energy Grant # DE-EE0002980.

REFERENCES

Bachmann, S., Y. Al-Rashid, P. Bronecke, R. Palmer, and B. Isom, 2010a: Suppression of the windfarm contribution from the atmospheric radar returns. *Electronic Proceedings for the 26th Conf. on IIPS*, Atlanta, GA.

Bachmann, S., Y. Al-Rashid, B. Isom, and R. Palmer, 2010b: Radar and windfarms - mitigating negative effects through signal processing. *the 6th European Conf. on Radar in Meteorology and Hydrology (ERAD)*, Sibiu, Romania.

Butler, M. and D. Johnson, 2003: Feasibility of mitigating the effects of windfarms on primary radar. *Alenia Marconi Systems Limited*.

DOE, 2008: 20% wind energy by 2030, report from the Energy Efficiency and Renewable Energy.

Greving, G., W. Biermann, and R. Mundt, 2007: Wind turbines and radar - the radar cross section rcs a useful figure for safeguarding. *Int. Radar Symposium (IRS)*, Cologne, Germany.

Greving, G. and M. Malkomes, 2008: Weather radar and wind turbines - theoretical and numerical analysis of the shadowing effects and mitigation concepts. *The 5th European Conf. on Radar in Meteorology and Hydrology (ERAD)*, Helsinki, Finland.

Isom, B., et al., 2008: Detailed observations of wind turbine clutter with scanning weather radars. *J. Atmos. Oceanic Technol.*, **26**, 894–910.

Kent, B., et al., 2008: Dynamic radar cross section and radar doppler measurements of commercial general electric windmill power turbines part 1: Predicted and measured radar signatures. *IEEE Antennas and Propagation Magazine*, **50**.

Nai, F., R. Palmer, and S. Torres, 2011: Wind turbine clutter mitigation using range-doppler domain signal processing method. *Preprints, 27th Conf. on Interactive Inform. and Proc. Sys. (IIPS)*, Seattle, WA.

Perry, J. and A. Biss, 2007: Wind farm clutter mitigation in air surveillance radar. *IEEE Aerospace Electron. Syst. Mag.*, **22**, 35–40.

Poupart, G., 2003: Wind farms impact on radar aviation interests final report, qinetiQ Contractor Reps. FES W/14/00614/00/REP and DTI PUB URN 03/1294.

TheWindPower, 2010: Available: http://www.thewindpower.net/statistics_ north_ america.php.

Vogt, R., T. Crum, M. Sandifer, E. Ciardi, and R. Guenther, 2009: A way forward wind farm - weather radar coexistence. *Wind Power Conference*, Chicago, IL.

Vogt, R., J. Reed, T. Crum, J. Snow, R. Palmer, and B. Isom, 2007a: Impacts of wind farms on wsr-88d operations and policy considerations. *Preprints, 23rd Int. Conf. on IIPS for Meteorology, Oceanography, and Hydrology*, San Antonio, TX.

Vogt, R., et al., 2007b: Weather radars and wind farms - working together for mutual benefit. *Extended Abstracts, WINDPOWER Conf. and Exhibition*, Los Angeles, CA.

Warde, D. and S. Torres, 2009: Automatic detection and removal of ground clutter contamination on weather radars. *Preprints, 34th Int. Conf. on Radar Meteorology*, Williamsburg, VA.

Webster, D., 2005: The effects of wind turbine farms on atc radar, aWC/WAD/72/665/TRIALS, AirWarfare Center, Waddington, United Kingdom.